*Erosion Prediction in Ungauged Basins: Integrating Methods and Techniques* (Proceedings of symposium HS01 held during IUGG2003 at Sapporo, July 2003). IAHS Publ. no. 279, 2003.

# First-order analysis of overland flow buffering in an ungauged fragmented upland basin

**ALAN D. ZIEGLER & THOMAS W. GIAMBELLUCA**
*Geography, University of Hawaii, Honolulu Hawaii 96822, USA*
adz@hawaii.edu

**Abstract** We investigate the degree to which the current juxtaposition of land cover in a fragmented basin in northern Vietnam mitigates the impacts of accelerated overland flow by buffering surface runoff generated on upslope source areas. Our methodology utilizes: (a) field measurements of infiltration-related soil properties, especially saturated hydraulic conductivity ($K_s$); (b) minute-by-minute rainfall data; (c) GIS analyses of land-cover distribution and flow-transitions between 30 × 30 m grid cells of major basin land covers; and (d) diagnostic simulations of overland flow generation using KINEROS2. We compare simulated basin-wide Horton overland flow (BWHOF) for the current land cover arrangement with that of three fragmentation scenarios: maximum buffering, minimum buffering, and random distribution of land-cover grid cells. The comparisons show that buffering opportunities for the current land-cover distribution are in between maximum and minimum buffering scenarios, and there are fewer buffering opportunities than for the situation where grid cells are distributed at random (i.e. a scenario representing a higher degree of fragmentation). The analyses support the idea that surface erosion and sediment delivery could be mitigated further if land covers having high $K_s$ were positioned intentionally below overland flow sources.

**Key words** forest fragmentation; KINEROS2; overland flow; southeast Asia; Vietnam

## INTRODUCTION

Fragmentation is a complex form of land-cover conversion in which large forest tracts are typically replaced by irregular (in shape and size) patches of forest and various "replacement" covers (Laurance & Bierregaard, 1997). The forest remnants are often disturbed both physically and ecologically; and the replacement covers may vary greatly in vegetative characteristics and usage. Compared with the original forested landscape, a fragmented basin is a mosaic of land covers differing in capability to infiltrate rainwater; and therefore, differing in the susceptibility to generate erosion-producing overland flow (Ziegler *et al*., 2003). In general, overland flow generation on fragmented lands is accelerated because of the abundance of disturbed surfaces with a high propensity to generate Horton overland flow (HOF, rainfall rate greater than infiltration and ponding; Horton, 1933). The juxtaposition of the various patches is important to basin-wide HOF production because patches of one particular land cover can conceivably buffer (via infiltration and physical blocking) HOF generated immediately upslope on source land covers. Substantial buffering could mitigate some of the geomorphological impacts of accelerated HOF generation; e.g. enhanced surface erosion, and sediment delivery to the stream.

Fragmented land cover has now replaced vast forests in many upland watersheds in southeast Asia, where erosion prediction is often hindered because many basins are

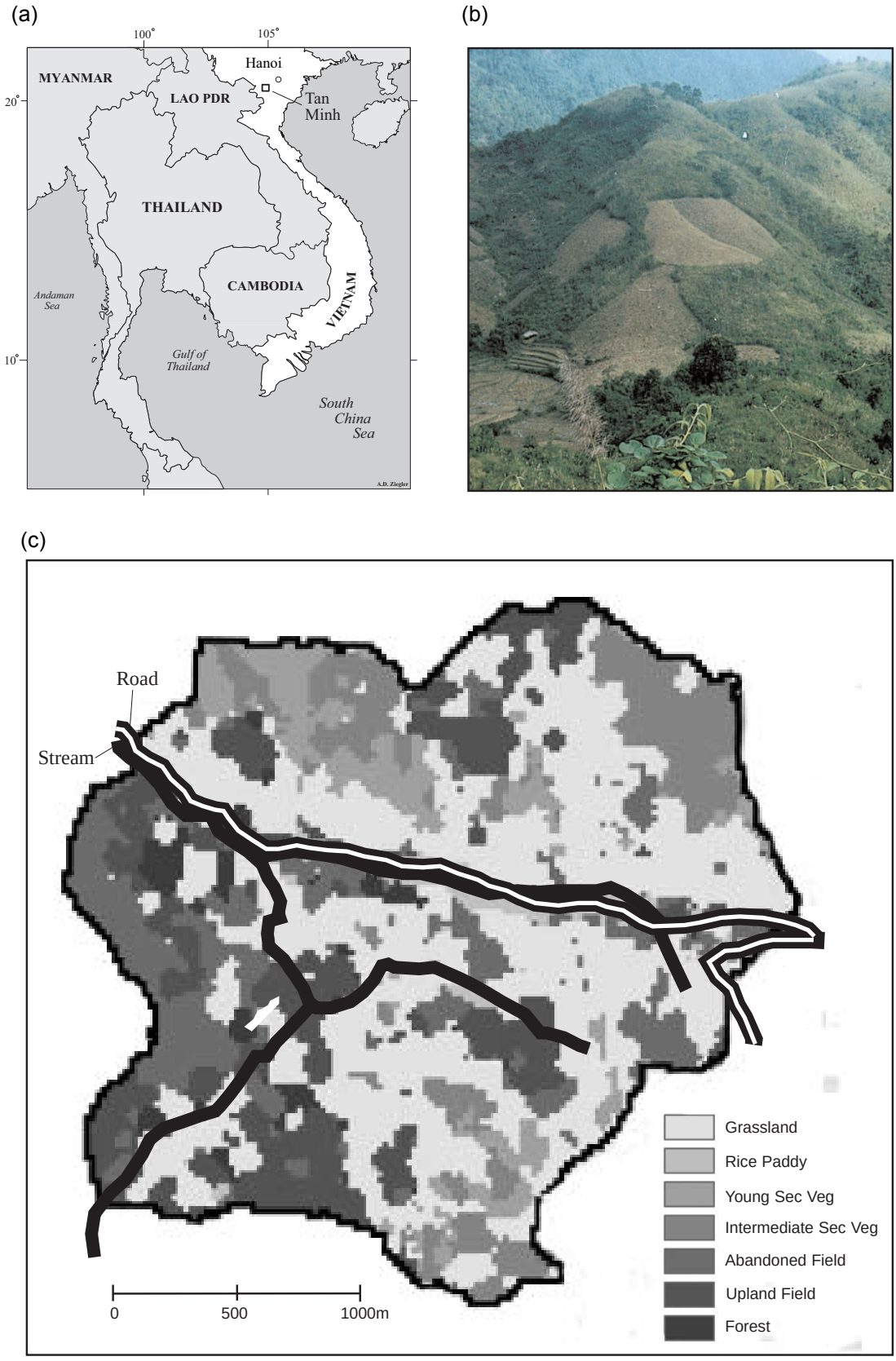


**Fig. 1** (a) Tanh Minh, the study area in northern Vietnam; (b) the fragmented landscape in Tanh Minh; (c) land-cover distribution in the 910-ha study watershed.

ungauged. Also, historical stream flow or sediment-related data are rarely available to compare with contemporary measurements or to use in the validation of distributed runoff-erosion models. In this paper, we use a simple diagnostic technique to estimate basin-wide HOF generation in an ungauged fragmented basin in northern Vietnam. In an attempt to understand the realm of hydrological and geomorphic impacts associated with land-cover change in the basin, we compare the current situation with three scenarios representing different degrees of fragmentation. Although this initial analysis focuses on runoff response, not erosion *per se*, we make inferences about the influence of fragmentation on surface erosion and sediment delivery.

## STUDY AREA

We focus on a 910-ha watershed that encompasses Tanh Minh Village, located SSW of Hanoi, in northern Vietnam (roughly 19°00′N, 104°45′E; Fig. 1(a)). Elevation ranges from 350 to 950 m a.s.l. Steep mountain slopes (30–60°) extend down to the valley floor. Parent bedrock material is largely sandstone and schist; soils are predominantly Ultisols. Approximately 90% of an annual 1800 mm of monsoon rainfall falls between May and October. Today, remnant forest patches exist primarily on steep, inaccessible peaks, ridges, and runs (Fig. 1(b)). Mountain slopes are dotted with active cultivated fields that are farmed by Tay villagers, the primary inhabitants. Typical swidden fields range in size from approximately 500 $m^2$ to more than 1 ha. Soil loss estimates made in 1995–1996 on cultivated and fallow fields range from about 40–180 Mg $ha^{-1}$ (Tran Duc Vien, unpublished data). In some locations, fields extend down to the riparian zone. In other locations, fields are bounded below by vegetated land covers, which potentially function as buffers of overland flow and transported sediment. Buffering, however, does not appear to be an intentional practice in Tanh Minh.

## METHODS

### Land-cover classification

Land-cover distribution was determined using a supervised classification (employing the maximum likelihood classifier algorithm in the ERDAS *Imagine* GIS) of a 7 November 1998 Landsat Thematic Mapper (TM) multi-spectral image (Fox *et al*., 2001). We identified eight major land covers in the study basin: rice paddy (RP), upland fields (UF), abandoned fields (AF), young secondary vegetation (YSV), grassland (GL), intermediate secondary vegetation (ISV), forest (F), and consolidated surfaces (CS). Vegetation descriptions are presented elsewhere (Ziegler *et al*., 2003). Although roads and paths are important sources of HOF, we do not include them in this analysis. We exclude rice paddies because we are focusing on the interaction of "hillslope surfaces"; paddy fields are functionally part of the stream system, and typically are located in valley bottoms.

## Spatial analysis

To derive the corresponding topography, the land-cover classification (30-m pixel resolution) was draped over a 30-m digital elevation model (DEM). The DEM was derived via ArcInfo version 7.3.1 (ESRI, Inc.) from a triangulated irregular network (TIN), which was constructed from a topographic map having a 20-m contour interval. Through spatial analysis of land cover and topography we derive the following variables related to overland flow pathways and buffering phenomena: (a) patch size (groups of contiguous cells having the same land-cover type); (b) flow direction from each DEM grid cell; and (c) flow-transition matrices (e.g. number of cells flowing from one land cover to another).

## Diagnostic simulations of basin-wide HOF

We conducted diagnostic computer simulations using the physics-based KINEROS2 runoff model (Smith *et al*., 1999) to determine the HOF generated by all transitions between each of six typical hillslope land covers (i.e. a total of 36 simulations for each storm). The simulated storm events are based on one-minute rainfall data collected with tipping-bucket raingauges during the period 26 March to 29 June 1998. For the seven largest storms, we simulated the HOF generated on, and transported through, adjacent upslope and downslope grid cells (this depth is referred to as $HOF_{storm}$). The dimensions of the two simulated surfaces are 30 × 30 m, matching those of the DEM. We use a constant slope value of 0.84 m $m^{-1}$ for each simulated surface. Important surface-specific model parameters are based on field-measured physical properties—notably saturated hydraulic conductivity ($K_s$), soil texture, porosity, canopy interception, percentage of vegetation coverage, and surface roughness. Data collection and model testing are described elsewhere (Ziegler *et al*., 2004).

As an index of HOF buffering potential, we estimate the basin-wide Horton overland flow generated during storms for any particular arrangement of grid cells with the following equation:

$$BWHOF_{scenario} = \frac{1}{N} \sum_{u=1}^{6} \sum_{d=1}^{6} T_{u,d} * H_{u,d} \quad (1)$$

where $T$ is a 6 × 6 land-cover transition matrix containing the number of upslope grid cells of land cover $u$ that flow into downslope grid cells of land cover $d$; $H$ is a 6 × 6 matrix of $HOF_{storm}$ values for every combination of six upslope and downslope landcovers; * refers to standard multiplication; and $N$ is the total number of land-cover transitions in the basins. Thus, *BWHOF* is a weighted mean of the HOF produced by all land-cover transitions.

The purpose of equation (1) is not to simulate accurately the total volume of HOF transported to the stream—a volume we cannot validate because the basin is ungauged. Rather, we use *BWHOF* as an index to show how HOF generation is affected by a given juxtaposition of grid cells (some of which are sources of HOF, others buffers). This analysis is limited to shallow, unconcentrated overland flow (SUOF), the type of HOF simulated by KINEROS2. Unless otherwise stated, all discussion regarding HOF refers to SUOF.

## RESULTS AND DISCUSSION

### Distribution of HOF sources and buffers

Table 1 lists area-related statistics and median $K_s$ for the basin land covers. Of note are the following: (a) about 32% of the area is currently or was recently in swidden cultivation (UF or AF); (b) 44% of the basin is grassland, a cover that has one of the highest median $K_s$ value (93 mm $h^{-1}$); (c) only 3% of the basin is forest, the land cover that once dominated the basin; (d) the basin consists of 243 patches, with a mean area of 3.7 ha; and (e) $K_s$ ranges from 30–100 mm $h^{-1}$ on the various land covers. The basin is therefore a mosaic of surfaces varying both in the propensity to generate overland flow and the capability to infiltrate that which is generated upslope (Fig. 1(c)). Based largely on $K_s$, we recognize the following source and buffer land-cover categories: {AF, YSV} and {UF, ISV, GL, and F}, respectively. Again, we do not consider rice paddies.

Our general premise is that if patches of land cover having high $K_s$ (buffers) are situated immediately downslope of HOF-producing source areas (low $K_s$), then the total volume of basin-wide HOF will be reduced. The land-cover transition matrix in Table 2(a) shows that only a small percentage of cell transitions for the current distribution are from sources (AF and YSV) to potential buffers (UF, ISV, GL, and F), suggesting that more erosion-producing overland flow may reach the streams in Tanh Minh than would be the case if buffers were intentionally situated below sources. It may also suggest that a higher degree of fragmentation would provide additional buffering. In particular, basin-wide HOF might be reduced if large source patches were converted into variety of smaller patches, some being composed of buffer land covers.

**Table 1** Area coverage, patch-related statistics, and median saturated hydraulic conductivity ($K_s$) values for major land covers in the study watershed.

| Land cover | Id | Area (ha) | Area (%) | Patch total | Mean patch area (ha) | Median $K_s$ (mm $h^{-1}$) |
|---|---|---|---|---|---|---|
| Upland field | UF | 162 | 17.8 | 44 | 3.7 | 103 |
| Abandoned field | AF | 126 | 13.9 | 68 | 1.9 | 28 |
| Grasslands | GL | 398 | 43.7 | 26 | 15.3 | 93 |
| Young secondary vegetation | YSV | 71 | 7.8 | 36 | 2.0 | 32 |
| Intermediate secondary vegetation | ISV | 98 | 10.8 | 29 | 3.4 | 67 |
| Forest | F | 25 | 2.8 | 24 | 1.0 | 63 |
| Rice paddy | RP | 30 | 3.3 | 16 | 1.9 | na |
| Total | | 910 | 100 | 243 | 3.7 | na |

### Basin-wide HOF for fragmentation scenarios

Table 3 compares basin-wide HOF (estimated via equation (1)) during seven storms for the current degree of fragmentation ($BWHOF_{current}$) with three fragmentation scenarios: (1) minimum buffering ($BWHOF_{min\text{-}buffering}$); (2) maximum buffering ($BWHOF_{max\text{-}buffering}$); and (3) land-cover cells are distributed at random ($BWHOF_{random}$). Land-cover transition matrices for the four scenarios are presented in Table 2. Because

**Table 2** Land-cover transition matrices listing the number of cells of one hillslope land cover that flow into cells of similar or different land cover for: (a) the current land-cover distribution, and for the scenarios of (b) maximum buffering, (c) minimum buffering, and (d) random distribution of grid cells.

(a) **Current distribution**

| | AF | YSV | UF | ISV | F | GL |
|---|---|---|---|---|---|---|
| AF | 1032 | 2 | 13 | 167 | 0 | 190 |
| YSV | 2 | 559 | 1 | 9 | 82 | 131 |
| UF | 28 | 0 | 190 | 21 | 0 | 40 |
| ISV | 115 | 1 | 19 | 1453 | 2 | 211 |
| F | 0 | 114 | 3 | 3 | 852 | 118 |
| GL | 163 | 95 | 53 | 188 | 81 | 3839 |

(b) **Maximum buffering**

| | AF | YSV | UF | ISV | F | GL |
|---|---|---|---|---|---|---|
| AF | 0 | 0 | 0 | 0 | 1404 | 0 |
| YSV | 0 | 0 | 0 | 0 | 0 | 784 |
| UF | 0 | 0 | 811 | 0 | 0 | 279 |
| ISV | 0 | 0 | 279 | 0 | 0 | 0 |
| F | 0 | 0 | 0 | 279 | 0 | 1522 |
| GL | 1404 | 784 | 0 | 0 | 397 | 1834 |

(c) **Minimum buffering**

| | AF | YSV | UF | ISV | F | GL |
|---|---|---|---|---|---|---|
| AF | 620 | 784 | 0 | 0 | 0 | 0 |
| YSV | 755 | 0 | 29 | 0 | 0 | 0 |
| UF | 0 | 0 | 0 | 279 | 232 | 579 |
| ISV | 0 | 0 | 0 | 0 | 0 | 279 |
| F | 29 | 0 | 1060 | 0 | 390 | 322 |
| GL | 0 | 0 | 1 | 0 | 1179 | 3239 |

(d) **Random distribution**

| | AF | YSV | UF | ISV | F | GL |
|---|---|---|---|---|---|---|
| AF | 202 | 113 | 157 | 40 | 259 | 635 |
| YSV | 113 | 63 | 87 | 22 | 144 | 354 |
| UF | 157 | 87 | 122 | 31 | 201 | 493 |
| ISV | 40 | 22 | 31 | 8 | 51 | 126 |
| F | 259 | 144 | 201 | 51 | 332 | 814 |
| GL | 635 | 354 | 493 | 126 | 814 | 1997 |

**Table 3** Characteristics for measured storms and corresponding basin-wide predicted HOF.

| Storm rank† | | 1 | 2 | 3 | 4 | 5 | 6 | 7 |
|---|---|---|---|---|---|---|---|---|
| Storm characteristics | | | | | | | | |
| Duration | (min) | 686 | 455 | 136 | 542 | 86 | 389 | 48 |
| Depth | (mm) | 66.8 | 28.7 | 30.7 | 38.6 | 18.3 | 21.8 | 14.2 |
| $I_{1\_MAX}$ | (mm $h^{-1}$) | 107 | 76 | 73 | 76 | 61 | 122 | 122 |
| $I_{30\_MAX}$ | (mm $h^{-1}$) | 57 | 32 | 32 | 31 | 31 | 26 | 25 |
| HOF scenarios | | | | | | | | |
| $BWHOF_{current}$ | (mm) | 1.46 | 0.05 | 0.10 | 0.20 | 0.02 | 0.13 | 0.10 |
| $BWHOF_{max\text{-}buffering}$ †† | (%) | –35.3 | –26.8 | –27.0 | –23.5 | –20.1 | –58.2 | –19.0 |
| $BWHOF_{min\text{-}buffering}$ †† | (%) | 16.7 | 13.0 | 20.3 | 7.6 | 4.6 | 25.2 | 6.9 |
| $BWHOF_{random}$ †† | (%) | –22.8 | –17.7 | –16.1 | –16.2 | –11.2 | –25.6 | –19.6 |

† $I_{1\_MAX}$ and $I_{30\_MAX}$ refer to maximum 1- and 30-min rainfall intensities; storms are ranked according to $I_{30\_MAX}$ values.

†† $BWHOF_{min\text{-}buffering}$, $BWHOF_{max\text{-}buffering}$, and $BWHOF_{random}$ are reported as percentage changes from $BWHOF_{current}$; the land-cover transition matrices used to calculate *BWHOF* for each scenario (equation (1)) are listed in Table 2.

of space limitations, the seven $HOF_{storm}$ matrices (H) are not presented. In the three alternative scenarios, total basin area occupied by each land cover is the same as for the current situation; the distribution of grid cells, however, has been altered. For

minimum- and maximum-buffering scenarios, $BWHOF_{scenario}$ is estimated by an optimization process that manipulates the land-cover transition matrices (Table 2) to maximize $BWHOF_{min\text{-}buffering}$ and minimize $BWHOF_{max\text{-}buffering}$ for storm 1. During optimization, we use constraints to ensure that the number of transitions both into and out of a particular land cover equals the basin total for that land cover. Hence, no more than one grid cell flows into any one cell; this is also the case for the random distribution calculation, but not for the current distribution calculation. For the random scenario, transition values are assigned by multiplying the total number of grid cells of an upslope land cover by the percentage of the total basin area that is occupied by a downslope land cover.

## HOF buffering in the fragmented basin

The buffering effectiveness of the current land-cover distribution is between that of the minimum and maximum buffering situations. In the case of maximum buffering, basin-wide HOF is 19–58% lower for the seven simulated storms ($BWHOF_{max\text{-}buffering}$, Table 3). In contrast, if a minimum degree of buffering existed (e.g. this might manifest as more large patches of source-to-source transitions) the increase in basin-wide HOF is on the order of 5–25% ($BWHOF_{min\text{-}buffering}$, Table 3). The greatest depth of basin-wide HOF is generated when a high percentage of source-to-source transitions occur; the least, when no source-to-source transitions occur and source-to-buffer transitions are maximized (see matrices in Table 2(b and c). These calculations indicate that some buffering is provided by the current arrangement of land covers, but it is not optimal. The $BWHOF_{random}$ calculations show how additional buffering may occur for the case of a higher degree of fragmentation. In Table 3, $BWHOF_{random}$ values are negative, indicating more buffering than for the current land-cover arrangement. HOF generation is reduced, in part, because source-to-source transitions are fewer (Table 2(d)).

## Limitations to this approach

Our diagnostic simulations represent a first-order technique that is useful when the paucity of data prohibits use of more robust methods (e.g. physics-based distributed runoff-erosion models that can be validated with measured data). We have made assumptions about some important processes in these analyses. For example, we do not consider the influence of concentrated overland flow, which compared with SUOF, is more erosive, has a greater capacity to entrain sediment, and is more likely to pass through downslope buffers. We ignore the role of non-Hortonian overland flow mechanisms, such as return flow and saturation overland flow, but we believe it is possible that SUOF augmented by additions from these sources could be buffered effectively so long as the flow is not concentrated. Finally, our assessment of buffering effectiveness is based solely on infiltration, when in fact, filtering of flow and entrained sediments is achieved both through infiltration and physical blocking by the vegetation comprising the buffer.

## CONCLUSION

The diagnostic simulations demonstrate the potential role land-cover juxtaposition plays in affecting the downslope movement of erosion-producing HOF, which is accelerated in the fragmented basin (*vs* that of the forested basin prior to land-cover conversion). The current land-cover distribution is neither optimal in terms of buffering HOF, nor is it excessively detrimental by this index. In general, fewer buffering opportunities exist for the current land-cover distribution than for the case where patch sizes are smaller and fragmentation is greater. These results support the idea that HOF-related impacts (e.g. surface erosion, delivery of sediment to the stream) could be mitigated if land covers having relatively high $K_s$ were positioned intentionally below HOF sources. On long slopes, more than one buffer may be needed, and the placement of such buffers should include both riparian and upper hillslope locations. The results also suggest simply that a higher degree of fragmentation could achieve a similar effect. Although we stop short of calculating the extent to which buffering reduces soil loss within the fragmented landscape, we assert that the linkage with HOF reduction is clearly identifiable: i.e. a reduction in overland flow fosters a reduction in surface erosion and sediment delivery.

**Acknowledgments** Financial support was provided by a National Science Foundation grant (no. DEB-9613613). ADZ was supported in part by and EPA STAR fellowship. Jefferson Fox, Mike Nullet, Don Plondke and Steve Leisz contributed to this research.

## REFERENCES

Fox, J., Leisz, S., Dao Minh Truong, Rambo, A. T., Nghiem Phuong Tuyen & Le Trong Cuc (2001) Shifting cultivation without deforestation: a case study in the mountains of northwestern Vietnam. In: *Applications of GIS and Remote Sensing in Biogeography and Ecology* (ed. by A. C. Millington, S. J. Walsh, & P. E. Osborne), 289–307. Kluwer Academic Publishers, Boston, USA.

Laurance, W. F. & Bierregaard Jr, R. O. (1997) Preface: A crisis in the making. In: *Tropical Forest Remnants: Ecology, Management, and Conservation of Fragmented Communities* (ed. by W. F. Laurance & R. O. Bierregaard Jr), xi–xv. University of Chicago Press, Chicago, USA.

Horton, R. E. (1933) The role of infiltration in the hydrologic cycle. *Eos Trans. Am. Geophys. Un.* **14**, 446–460.

Smith, R. E, Goodrich, D. C. & Unkrich, C. L. (1999) Simulation of selected events on the Catsop catchment by KINEROS2: a report for the GCTE conference on catchment scale erosion models. *Catena* **37**, 457–475.

Ziegler, A. D., Giambelluca, T. W., Vana, T. T., Nullet, M. A., Fox, J., Vien, T. D. & Evett, S. (2003) Hydrological consequences of landscape fragmentation in mountainous Northern Vietnam: evidence of accelerated overland flow generation. *J. Hydrol*. (in press).

Ziegler, A. D., Giambelluca, T. W., Plondke, D., Leisz, S., Fox, J. & Truong, D. M. (2004) Hydrological consequences of landscape fragmentation in mountainous Northern Vietnam: buffering of accelerated overland flow. *Land Use and Water Resour. Res.* (submitted).